

# Fast Transient Simulations for Multi-Segment Transmission Lines with a Graphical Model

Joel B. Harley<sup>1, \*</sup>, Mashad U. Saleh<sup>2</sup>, Samuel Kingston<sup>2</sup>,  
Michael A. Scarpulla<sup>2</sup>, and Cynthia M. Furse<sup>2</sup>

**Abstract**—This paper studies a computationally efficient algebraic graph theory engine for simulating time-domain one-dimensional waves in a multi-segment transmission line, such as for reflectometry applications. Efficient simulation of time-domain signals in multi-segment transmission lines is challenging because the number of propagation paths (and therefore the number of operations) increases exponentially with each new interface. We address this challenge through the use of a frequency-domain, algebraic graphical model of wave propagation, which is then converted to the time domain via the Fourier transform. We use this model to achieve an exact, stable, and computationally efficient ( $\mathcal{O}(NQ)$ , where  $N$  is the number of segments and  $Q$  is the bandwidth) approach for studying one-dimensional wave propagation. Our approach requires the reflection and transmission coefficients for each interface and each segment's complex propagation constant. We compare our simulation results with known analytical solutions.

## 1. INTRODUCTION

This paper discusses the use of algebraic graph theory for simulating time-domain signals with multiple reflections in multi-segment transmission lines. We use multi-segment electrical transmission lines as an example, but the approach is generalizable to other modalities of one-dimensional wave propagation. For example, this simulation work could be applied to structural ultrasound [1, 2], medical ultrasound [3], or electrical diagnostics systems [4]. In these modalities, we often analyze one-dimensional wave propagation behavior to better understand the characteristics of waves traveling in complex structural, biological, and electrical systems [5].

Techniques such as spread spectrum time domain reflectometry [4, 6] transmit wideband signals into electrical transmission lines and measure reflection amplitudes and delays to detect and locate faults. Characterizing faults can often be accomplished by solving an inverse problem. Yet, for multi-segment transmission lines, solving these inverse problems often require a reliable and fast simulation engine.

In general, simulation techniques become less attractive as the transmission line grows and as more interfaces are added [7, 8]. For example, finite element [9], finite difference time domain [10], and transmission line matrix [11] models are very powerful but have several challenges. Specifically, these methods yield approximate solutions, and their stability depends on choosing appropriate spatial sampling or meshing parameters [12]. The transfer matrix [13] method represents an alternative approach for modeling wave propagation. In geophysics, optics, and acoustics, the transfer matrix method [14] represents the wave behavior across each segment with matrices. These matrices are multiplied together to determine the aggregate behavior. While this approach is reliable, the computational cost increases exponentially with the number of segments [15]. The computational

---

*Received 21 April 2019, Accepted 26 June 2019, Scheduled 5 August 2019*

\* Corresponding author: Joel B. Harley (joel.harley@ufl.edu).

<sup>1</sup> Department of Electrical and Computer Engineering, University of Florida, Gainesville, FL 32603, USA. <sup>2</sup> Department of Electrical and Computer Engineering, University of Utah, Salt Lake City, UT 84112, USA.

complexity of many grid or mesh based simulation methods scale with  $N$ , the number of voltage nodes/values in the model, and  $Q$ , the bandwidth of the signal [16]. For example, the finite element method [17] has a computational complexity of  $\mathcal{O}(NQ^2)$ . Yet, the number of nodes is often very large. For example, the finite difference time domain (FDTD) method requires a minimum density of 10 nodes per wavelength [18] to accurately simulate waves. This further increase computational costs.

As a result, we present a computationally efficient simulation engine based on knowledge of reflection and transmission coefficients and propagation coefficients (velocities and attenuations). We use an algebraic graphical model to derive our approach and demonstrate a computational complexity of  $\mathcal{O}(NQ)$ , where  $N$  is the number of graphical nodes, and  $Q$  is the bandwidth of the excitation signal. Unlike methods like FDTD,  $N$  only needs to be proportional to the number of segments or interfaces in the transmission line. The graphical model we use is similar to signal flow graphs in the microwave, control, and electromagnetics literature [19–22], where each node in the graph corresponds to voltages traveling in a known direction. In the signal processing literature, algebraic graph theory [23] has seen much research with studies into the interconnectedness of complex systems [24, 25]. In addition, advances in computing with large, sparse data sets [26, 27] has enabled computationally efficient methods for solving inverse problems in algebraic graph structures [28, 29].

From the perspective of algebraic graph theory, we demonstrate how graphs can efficiently model time-series information propagating in a one-dimensional transmission line. From the perspective of wave theory, we demonstrate a computationally efficient method for simulating wave propagation in multi-segment transmission lines. We prove that our approach has guaranteed convergence and stability. We also demonstrate that the simulations match theory.

## 2. BACKGROUND

In this section, we provide the necessary background for defining a multi-segment transmission line as an algebraic graphical model. We will use these concepts to create our simulation method. We also describe the theoretical reflection and transmission behavior with one and two interfaces. We will later demonstrate that our graphical model matches this theory.

We consider a multi-segment transmission line and all of its multi-path components, as illustrated in Fig. 1. That is, we consider a one-dimensional transmission line that can be divided into multiple segments, each with potentially different wave propagation characteristics. We define each segment by two quantities: its characteristic impedance  $Z_0(\omega)$  and complex propagation coefficient  $\gamma(\omega)$ . The characteristic impedance is a frequency-dependent measure of the ratio of the electric to magnetic fields in a transmission line. The propagation coefficient represents the complex frequency-dependent wavenumber/velocity and attenuation of a propagating wave. Note that the  $S$ -parameters for each interface (i.e., the reflection and transmission coefficients) are directly related to the characteristic impedances of the two adjoining segments.

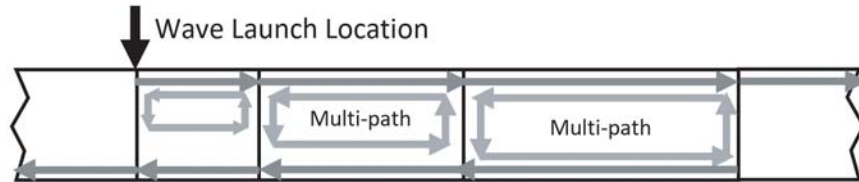


**Figure 1.** Illustration of a multi-segment transmission line with many paths that waves can travel. We assume the first and last segments are infinitely large.

### 2.1. Single Segment: Propagation

The propagation coefficient describes how waves travel in a segment, between two interfaces. We represent this in the frequency domain as

$$H(\omega) = e^{-\gamma(\omega)(\Delta d)},$$

where  $\Delta d$  is the travel distance across the segment. Note that, in general,  $\gamma(\omega)$  is composed of an imaginary part representing the wavenumber of the propagating wave, which controls the frequency-dependent phase shift, and a real part representing the attenuation of the propagating wave. When  $\gamma(\omega)$  is a purely imaginary value and linear with respect to frequency,  $H(\omega)$  corresponds to a time-delay.

### 2.2. Single Interface: Reflection and Transmission

We represent our transmission line as a series of sequential segments. The only sources of reflections are from the interfaces between segments. For example, consider an interface between two segments, labelled segment 0 and segment 1 (with characteristic impedances  $Z_0(\omega)$  and  $Z_1(\omega)$ , respectively). This is illustrated in Fig. 2(a). The reflection coefficient  $\Gamma_{0|1}(\omega)$  for a wave arriving from segment 0 can be described by

$$\Gamma_{0|1}(\omega) = \frac{Z_1(\omega) - Z_0(\omega)}{Z_1(\omega) + Z_0(\omega)}.$$

If we reverse the direction of propagation from the 0|1 direction to the 1|0 direction, we get the relationship

$$\Gamma_{1|0}(\omega) = -\Gamma_{0|1}(\omega).$$

Therefore, the reflection coefficient in either direction can be represented with one function.

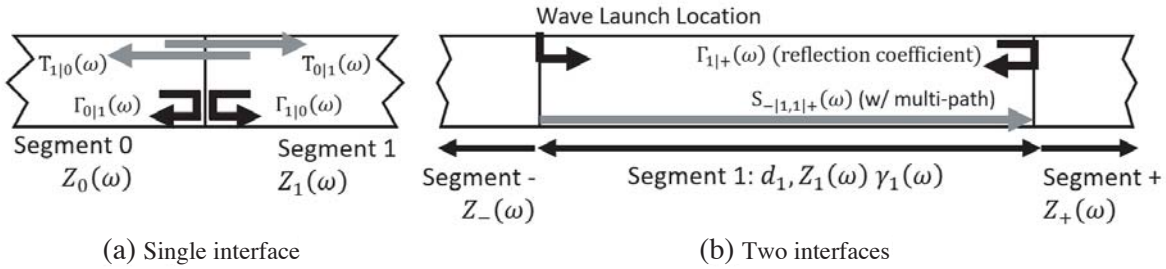


**Figure 2.** Illustration of a two-interface transmission line with labels illustrating different quantities used considered in our simulation engine. Note that we assume the first and last segment to be infinite in length.

Similarly, the transmission coefficient from segment 0 to 1 for the same interface (assuming no absorption at the interface) can be described by

$$T_{0|1}(\omega) = \frac{2Z_1(\omega)}{Z_1(\omega) + Z_0(\omega)} = 1 + \Gamma_{0|1}(\omega). \tag{1}$$

If we reverse the direction of propagation from the 0|1 direction to the 1|0 direction, we get the relationship

$$T_{1|0}(\omega) = 1 - \Gamma_{0|1}(\omega). \tag{2}$$

Therefore, the reflection and transmission coefficients for traveling in either direction across an interface can be expressed by the reflection coefficient  $\Gamma_{0|1}(\omega)$ .

### 2.3. Two Interfaces: Reflection, Transmission, and Propagation

When there are two interfaces, waves will reflect and propagate between both interfaces in a recursive manner. That is, reflections from one interface will reflect off another interface. In this subsection, we theoretically derive this behavior as an illustrative example. In our results section, we demonstrate that our graphical model produces the same result.

Consider a transmission line with two interfaces, as illustrated in Fig. 2(b). We consider three segments, labeled:  $-$ ,  $1$ , and  $+$  with two interfaces:  $-|1$  and  $1|+$ . In this notation,  $-|1$  implies the wave is travelling from segment  $-$  to segment  $1$  and  $1|+$  implies the wave is travelling from segment  $1$

to segment  $-$ . The  $-$  and  $+$  segments are considered infinitely long. As a result, the characteristic impedances  $Z_-(\omega)$  and  $Z_+(\omega)$  can be considered the output impedance and input impedance for the transmission line, respectively.

Given this model, we consider the effective transfer function  $S_{-|1,1|+}(\omega)$  corresponding to the sum of all waves originating at the  $-|1$  interface and traveling to the right and ending at the  $1|+$  interface. This transfer function is defined by

$$S_{-|1,1|+}(\omega) = e^{-\gamma_1(\omega)d_1} + e^{-\gamma_1(\omega)d_1} \left( \Gamma_{1|-}(\omega)\Gamma_{1|+}(\omega)e^{-\gamma_1(\omega)2d_1} \right) + e^{-\gamma_1(\omega)d_1} \left( \Gamma_{1|-}(\omega)\Gamma_{1|+}(\omega)e^{-\gamma_1(\omega)2d_1} \right)^2 + \dots = e^{-\gamma_1(\omega)d_1} \sum_{n=0}^{\infty} \left[ \Gamma_{1|-}(\omega)\Gamma_{1|+}(\omega)e^{-\gamma_1(\omega)2d_1} \right]^n \quad (3)$$

where  $\gamma_1(\omega)$  and  $d_1$  are the propagation coefficient and length of segment 1, respectively. The terms represent propagation and reflection in the first segment, followed by the reflections recursively traveling a distance of  $2d_1$  between the  $1|+$  and  $-|1$  interfaces. The term  $n$  represents the number of times the wave has traveled across the segment.

This transfer function, or effective reflection coefficient, can be simplified by applying the definition of a geometric series such that

$$S_{-|1,1|+}(\omega) = \frac{e^{-\gamma_1(\omega)d_1}}{1 + \Gamma_{-|1}(\omega)\Gamma_{1|+}(\omega)e^{-\gamma_1(\omega)2d_1}}, \quad (4)$$

where we use the property that  $\Gamma_{-|1}(\omega) = -\Gamma_{1|-}(\omega)$  to standardize the reflection coefficient notation to correspond to waves traveling from left-to-right (i.e., the forward direction). This form demonstrates that the effective transmission coefficient has a direct term (the numerator) and a recursive term (the denominator). Note that this expression is guaranteed to be stable (i.e., the time domain response converges to zero) as long as  $\Gamma_{1|+}(\omega) < 1$ ,  $\Gamma_{-|1}(\omega) < 1$ , and  $\Re\{\gamma(\omega)\} \geq 0$  for all  $\omega$ . This always holds true in practical transmission line scenarios.

While this approach nicely models the infinite number of reflections between two interfaces, it is not trivial to extend the closed-form solution to more than two interfaces. In the following section, we build an extension of this concept through the use of an algebraic graphical model and linear algebra. While the underlying mathematics is different, the overall derivation process is similar.

### 3. GRAPHICAL MODEL OF WAVE PROPAGATION

#### 3.1. Graph Representation

We represent the transmission line with a directed graph  $\mathcal{G} = \{\mathcal{V}, \mathcal{E}\}$ . The graph contains vertices (or nodes)  $v_n \in \mathcal{V}$  and edges that connect the nodes  $\epsilon_{ij} \in \mathcal{E}$ . Each node has a frequency-dependent value, which represents the frequency-dependent voltage in a transmission line before or after an interface. The edges connect nodes and possess complex weights. When a value (i.e., wave voltage) travels between nodes via an edge, the source node value  $v_n$  is multiplied by the edge weight  $\epsilon_{ij}$  and then placed into the destination node. This process, known as a graph shift [30], occurs simultaneously for all nodes.

Figure 3 illustrates two-interface and three-interface systems and their corresponding graphical models. The values next to each edge correspond to the fixed edge weights. These complex values represent the reflection coefficients, transmission coefficients, and propagation delays in the frequency domain. We assume an output impedance  $Z_-(\omega)$  (i.e., the impedance of the left-most, infinitely long segment) and input impedance  $Z_+(\omega)$  (i.e., the impedance of the right-most, infinitely long segment). Each segment has a characteristic impedance  $Z_i(\omega)$ , propagation constant  $\gamma_i(\omega)$ , and length  $d_i$  for all  $i$ .

This model is similar to signal flow graphs found in the microwaves, control, and electromagnetics literature [19–22]. That is, the graphical model describes how voltage flows from one part of the transmission line to another. The nodes at the top of the graph correspond to forward traveling waves, and the nodes at the bottom correspond to backward traveling waves. Each node contains a direction-dependent voltage at one side of a boundary or interface. The sum of the vertically aligned nodes represents the voltage at that location.

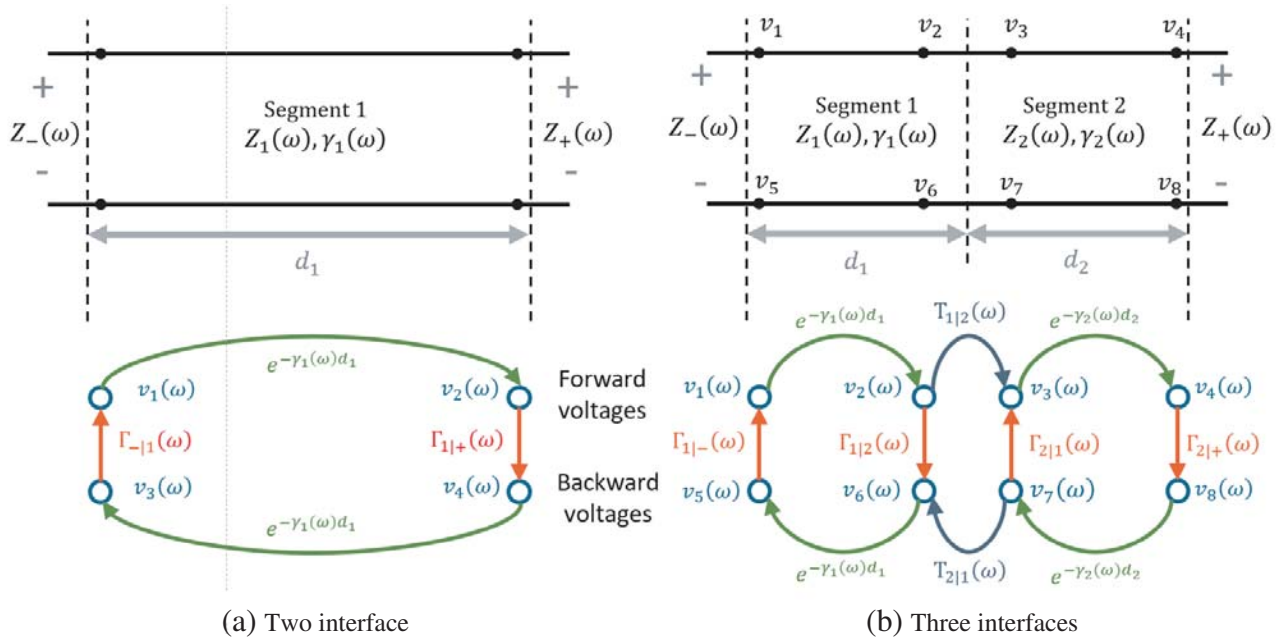


**Figure 3.** Illustration of a graphical model for (a) a two-interface transmission line and (b) a three-interface transmission line. Each node in the graphical model represents one immediate side of a boundary, where we can generate or measure waves. The value (e.g., voltage) in each node is multiplied by the edge weights as they travel throughout the graph.

Each edge indicates how the wave travels across a homogeneous transmission line segment or how the wave changes at an interface. Horizontal lines represent transmission across a segment or interface. Vertical lines represent reflection at an interface. Hence, a vertical line transitions forwarding-traveling voltages into backward-traveling voltages or vice-versa. This allows us to model multiple reflections in the transmission line. Each edge has a complex frequency-dependent weight corresponding to a transmission coefficient, reflection coefficient, or phase shift.

Through the graph, the wave propagation is represented by a dynamical model. That is, we specify a relationship between each node at frequency  $\omega$  by

$$\mathbf{v}^{(i)}(\omega) = \mathbf{A}(\omega)\mathbf{v}^{(i-1)}(\omega) \tag{5}$$

where  $\mathbf{A}(\omega)$  is an adjacency matrix,  $\mathbf{v}^{(i)}(\omega)$  represents a vector of node values (i.e., all forward and backward traveling waves voltages) at step  $i$ ,

$$\mathbf{v}^{(i)}(\omega) = \left[ v_1^{(i)}(\omega) \quad \dots \quad v_N^{(i)}(\omega) \right]^T, \tag{6}$$

where  $1 \leq n \leq N/2$  corresponds to nodes with forward traveling values, and  $N/2 + 1 \leq n \leq N$  corresponds to nodes with backward traveling values. Hence,  $v_1^{(i)}(\omega) + v_{N/2+1}^{(i)}(\omega)$  represents the total voltage at node 1 during step  $i$ . These nodes are illustrated in Fig. 3. Note that alternative ordering of the nodes can be used. Also note that the order of steps corresponds to an order of events but does not explicitly correspond to time. Instead, time is encoded through the frequency-domain phase shifts, i.e.,  $e^{-\gamma(\omega)d}$ .

### 3.2. The Wave Adjacency Matrix

For a general graph, the weighted adjacency matrix that represents the connections between nodes is expressed by an  $N \times N$  block matrix

$$\mathbf{A}(\omega) = \begin{bmatrix} \mathbf{T}_+(\omega) & \mathbf{R}_+(\omega) \\ \mathbf{R}_-(\omega) & \mathbf{T}_-(\omega) \end{bmatrix} \tag{7}$$

The  $(N/2) \times (N/2)$  submatrices correspond to forward-traveling behavior  $\mathbf{T}_+(\omega)$ , backward-traveling behavior  $\mathbf{T}_-(\omega)$ , forward-to-backward reflection behavior  $\mathbf{R}_-(\omega)$ , and backward-to-forward reflection behavior  $\mathbf{R}_+(\omega)$ . The submatrices are specifically defined by

$$[\mathbf{T}_+(\omega)]_{ij} = \begin{cases} e^{-\gamma_k(\omega)d_k}, & k = i/2, \quad j = i - 1, \quad i \in \{2, 4, \dots, N/2\} \\ T_{k|k+1}(\omega), & k = (i - 1)/2, \quad j = i - 1, \quad i \in \{3, 5, \dots, N/2 - 1\} \\ 0, & \text{otherwise} \end{cases} \quad (8)$$

$$[\mathbf{T}_-(\omega)]_{ij} = \begin{cases} e^{-\gamma_k(\omega)d_k}, & k = i/2, \quad i = j - 1, \quad j \in \{2, 4, \dots, N/2\} \\ T_{k+1|k}(\omega), & k = (i - 1)/2, \quad i = j - 1, \quad j \in \{3, 5, \dots, N/2 - 1\} \\ 0, & \text{otherwise} \end{cases} \quad (9)$$

$$[\mathbf{R}_+(\omega)]_{ij} = \begin{cases} \Gamma_{1|-}(\omega), & i = j = 1 \\ \Gamma_{k+1|k}(\omega), & k = (i - 1)/2, \quad i \in \{3, 5, \dots, N/2 - 1\} \\ 0, & \text{otherwise} \end{cases} \quad (10)$$

$$[\mathbf{R}_-(\omega)]_{ij} = \begin{cases} \Gamma_{k|k+1}(\omega), & k = i/2, \quad i \in \{2, 4, \dots, (N - 1)/2\} \\ \Gamma_{N/2|+}(\omega), & i = j = N/2 \\ 0, & \text{otherwise} \end{cases} \quad (11)$$

where the notation  $[\mathbf{A}(\omega)]_{ij}$  denotes the  $i$ th row and  $j$ th column of  $\mathbf{A}(\omega)$ . Note that  $d_k$  is strictly positive in this setup. As mentioned in the previous section, all of the transmission and reflection coefficients can be written in terms of forward-travelling reflection coefficients. Therefore, for the three-interface example illustrated in Fig. 3(b), the corresponding matrices are expressed as

$$\mathbf{T}_+(\omega) = \begin{bmatrix} 0 & 0 & 0 & 0 \\ e^{-\gamma_1(\omega)d_1} & 0 & 0 & 0 \\ 0 & 1 + \Gamma_{1|2}(\omega) & 0 & 0 \\ 0 & 0 & e^{-\gamma_2(\omega)d_2} & 0 \end{bmatrix} \quad (12)$$

$$\mathbf{T}_-(\omega) = \begin{bmatrix} 0 & e^{-\gamma_1(\omega)d_1} & 0 & 0 \\ 0 & 0 & 1 - \Gamma_{1|2}(\omega) & 0 \\ 0 & 0 & 0 & e^{-\gamma_2(\omega)d_2} \\ 0 & 0 & 0 & 0 \end{bmatrix} \quad (13)$$

$$\mathbf{R}_+(\omega) = \begin{bmatrix} -\Gamma_{-|1}(\omega) & 0 & 0 & 0 \\ 0 & 0 & 0 & 0 \\ 0 & 0 & -\Gamma_{1|2}(\omega) & 0 \\ 0 & 0 & 0 & 0 \end{bmatrix} \quad (14)$$

$$\mathbf{R}_-(\omega) = \begin{bmatrix} 0 & 0 & 0 & 0 \\ 0 & \Gamma_{1|2}(\omega) & 0 & 0 \\ 0 & 0 & 0 & 0 \\ 0 & 0 & 0 & \Gamma_{2|+}(\omega) \end{bmatrix} \quad (15)$$

Figure 4 illustrates the absolute value of the adjacency matrix for  $N = 80$  nodes or, equivalently, 20 segments. The image shows that the matrix is highly sparse and very structured. As a result of this sparsity and structure, the matrix can be constructed relatively quickly.

### 3.3. Numerical Simulation with Graphical Model

The adjacency matrix represents the transition between values at our previous state  $\mathbf{v}^{(i-1)}(\omega)$  and our current state  $\mathbf{v}^{(i)}(\omega)$ . This transition includes all time/phase delays in the form of multiplications with complex frequency-domain exponentials. Note that while each step represents an ordered event, it does not represent actual time. Therefore the final signal we observe is represented by the sum of all steps (from 0 to  $\infty$ ) through the graph.

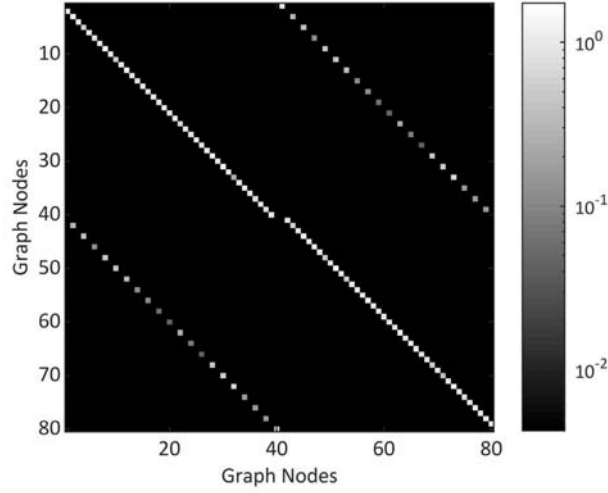


**Figure 4.** Example of an 80-node/20-segment adjacency matrix. The image demonstrates the significant sparsity of the matrix.

Mathematically, if  $\mathbf{v}^{(0)}(\omega)$  represents the initial conditions (including direction), then wave events progress according to

$$\mathbf{v}^{(i)}(\omega) = \mathbf{A}^i(\omega)\mathbf{v}^{(0)}(\omega) \tag{16}$$

To incorporate all reflections and transmissions in our model, we sum the results over all steps,

$$\mathbf{v}(\omega) = \sum_{i=0}^{\infty} \mathbf{A}^i(\omega)\mathbf{v}^{(0)}(\omega) \tag{17}$$

This can then be simplified through application of the Neumann series (the matrix equivalent of the geometric series), which states that

$$\sum_{k=0}^{\infty} \mathbf{A}^k(\omega) = (\mathbf{I} - \mathbf{A}(\omega))^{-1}, \tag{18}$$

where  $\mathbf{I}$  is the identity matrix. When this expression is used, the sum can be represented as

$$\mathbf{v}(\omega) = [\mathbf{I} - \mathbf{A}(\omega)]^{-1} \mathbf{v}^{(0)}(\omega). \tag{19}$$

Hence, we are able to compute the infinite sum as a matrix inverse. The resulting matrix

$$\mathbf{S}(\omega) = [\mathbf{I} - \mathbf{A}(\omega)]^{-1} \tag{20}$$

corresponds to the transfer function between any two nodes. That is,  $\mathbf{S}(\omega)$  at row  $i$  and column  $j$  represents the transfer function for waves starting at node  $j$  and ending at node  $i$ .

### 3.4. Time-Domain Calculation

Each element of  $\mathbf{S}(\omega)$  corresponds to a frequency-domain transfer function. To compute the associated time-domain impulse responses from any of these frequency-domain responses, we first sample frequencies according to

$$f_q = \left(\frac{q}{Q}\right) F_s \quad \text{for} \quad -\left\lfloor \frac{Q}{2} \right\rfloor \leq q \leq \left\lfloor \frac{Q-1}{2} \right\rfloor,$$

where  $\lfloor Q/2 \rfloor$  denotes the floor operation;  $F_s$  is the desired sampling rate in time; and  $Q$  is the number of frequencies. The variable  $q$  represents each frequency used in the simulation. To get the time-domain signal, we compute the inverse fast Fourier transform of the simulated values at those frequencies. Note that if  $Q$  is not sufficiently large, we may observe significant temporal aliasing.

### 3.5. Solution Convergence

In general, the Neumann series is valid if and only if the underlying dynamical system  $\mathbf{v}^{(i)}(\omega) = \mathbf{A}^{(i)}(\omega)\mathbf{v}^{(i-1)}(\omega)$  approaches the vector  $\mathbf{0}$  as  $i \rightarrow \infty$ . To demonstrate that our method satisfies this condition, we observe that a graphical dynamical system approaches  $\mathbf{0}$  as  $i \rightarrow \infty$  when every set of nodes and edges in a graph cycle  $\mathcal{C}$  satisfies

$$\left| \prod_{i \in \mathcal{C}} \epsilon_i \right| < 1, \quad (21)$$

where  $\epsilon_i$  is each edge weight in the cycle  $\mathcal{C}$ .

To understand this, recognize that (assuming that each weight is  $\epsilon_i < \infty$ ) the node values in a directed graph can only grow non-stop through some recursive process (i.e., a graph cycle). As wave amplitudes travel along the cycle, they are multiplied by the weights in that cycle. Therefore, if the weights of every cycle reduce the strength of the initial input condition (i.e., the magnitude of the product is  $< 1$ ), then the values in each node will converge to zero.

Any cycle in the graph will contain pairs of reflection coefficients, pairs of propagation coefficients, and pairs of transmission coefficients. Due to the conservation of energy, we know that the reflection coefficients and propagation coefficients satisfy  $|\Gamma_{ij}(\omega)| < 1$  and  $|e^{-\gamma_m(\omega)d_m}| < 1$  for every node pair  $i, j$  and every segment  $m$ . When  $\Gamma_{ij}(\omega)$  is negative, the transmission coefficients can be greater than one. However, every cycle must contain a forward transmission coefficient  $T_{a|b}(\omega) = 1 + \Gamma_{a|b}(\omega)$  and an associated backward transmission coefficient  $T_{b|a}(\omega) = 1 - \Gamma_{b|a}(\omega)$ . The product of these values is

$$T_{a|b}(\omega)T_{b|a}(\omega) = (1 + \Gamma_{a|b}(\omega))(1 - \Gamma_{a|b}(\omega)) \quad (22)$$

$$= 1 - \Gamma_{a|b}^2(\omega) \quad (23)$$

$$< 1 \quad (24)$$

Hence, the product of all coefficients in a cycle must be less than one. As a result, our numerical method converges to an exact solution for any initial condition  $\mathbf{v}^{(0)}(\omega)$ .

### 3.6. Computational Complexity

Our graphical solution in Equation (19) is computed by solving a highly sparse system (i.e., most coefficients are zero) of linear equations,  $\mathbf{I} - \mathbf{A}(\omega)$ . Solving sparse linear systems has been a topic of significant research [31, 32] because it allows us to solve very large computational problems with great computational and storage efficiency. In general, sparse linear system solvers can achieve a  $\mathcal{O}(N)$  computational complexity, where  $N$  is the number of nodes in the graph. As a reference, traditional matrix inversion has  $\mathcal{O}(N^3)$  computational complexity. Filling the inverse matrix with an assumed known (and dense) closed-form solution has a computational complexity of  $\mathcal{O}(N^2)$ .

We solve this system of equations for each frequency. Therefore, the computational complexity across every frequency is  $\mathcal{O}(NQ)$ , where  $Q$  is the number of frequencies. However, we can decrease this computational complexity by considering only frequencies of importance. For example, a steady state excitation at 10 MHz only requires us to solve the system of linear equations for that frequency.

## 4. RESULTS AND EXAMPLES

In this section, we test and verify our simulation engine. We first verify that our engine's solution matches that of the two-interface transmission line in Section 2. We then demonstrate three examples of wave propagation in different multi-segment transmission lines. The first example simulates a frequency-dependent velocity and attenuation. The second example simulates multiple interfaces and multiple characteristic impedances. The third example simulates a spatially-dependent velocity (i.e., the velocities change across many small, individual segments). For each example, note that the real part of the propagation coefficient corresponds to attenuation, and the imaginary part of the propagation coefficient is equal to

$$\text{Im} \{ \gamma(\omega) \} = k(\omega) = \frac{\omega}{c(\omega)},$$

where  $k(\omega)$  is the wavenumber and  $c(\omega)$  is the phase velocity.

For demonstration purposes, we will simulate more interfaces than necessary (each that exhibit no change in impedance or propagation constant). This is done to illustrate how simulated waves spatially change. With the exception of the third example, this is not necessary for accurate time-domain simulations. It is necessary for the third example since the waves constantly change in space.

#### 4.1. Verifying Solution with Two Interfaces

In Section 2, we derived a reflection coefficient for two interfaces. In this subsection, we verify this result with our graphical approach. We derive the closed-form solution for the Neumann series and demonstrate that it achieves the same result.

When we consider the two interface problem, as shown in Fig. 3, the adjacency matrix can be expressed by

$$\mathbf{A}(\omega) = \begin{bmatrix} 0 & 0 & -\Gamma_-(\omega) & 0 \\ e^{-\gamma_1(\omega)d_1} & 0 & 0 & 0 \\ 0 & 0 & 0 & e^{-\gamma_1(\omega)d_1} \\ 0 & \Gamma_+(\omega) & 0 & 0 \end{bmatrix} \quad (25)$$

The closed-form expression for the Neumann Series solution with this adjacency matrix is expressed by

$$\begin{aligned} \mathbf{S}(\omega) &= [\mathbf{I} - \mathbf{A}(\omega)]^{-1} \\ &= \frac{\begin{bmatrix} S_{-|1,-|1}(\omega) & S_{1|+,-|1}(\omega) & S_{1|-,-|1}(\omega) & S_{+|1,-|1}(\omega) \\ S_{-|1,1|+}(\omega) & S_{1|+,1|+}(\omega) & S_{1|- ,1|+}(\omega) & S_{+|1,1|+}(\omega) \\ S_{-|1,1|-}(\omega) & S_{1|+,1|-}(\omega) & S_{1|- ,1|-}(\omega) & S_{+|1,1|-}(\omega) \\ S_{-|1,+|1}(\omega) & S_{1|+,+|1}(\omega) & S_{1|- ,+|1}(\omega) & S_{+|1,+|1}(\omega) \end{bmatrix}}{1 + \Gamma_-(\omega)\Gamma_+(\omega)e^{-\gamma_1(\omega)2d_1}} \\ &= \begin{bmatrix} 1 & -\Gamma_-(\omega)\Gamma_+(\omega)e^{-\gamma_1(\omega)d_1} & -\Gamma_-(\omega) & -\Gamma_-(\omega)e^{-\gamma_1(\omega)d_1} \\ e^{-\gamma_1(\omega)d_1} & 1 & -\Gamma_-(\omega)e^{-\gamma_1(\omega)d_1} & -\Gamma_-(\omega)e^{-\gamma_1(\omega)2d_1} \\ \Gamma_+(\omega)e^{-\gamma_1(\omega)2d_1} & \Gamma_+(\omega)e^{-\gamma_1(\omega)d_1} & 1 & e^{-\gamma_1(\omega)d_1} \\ \Gamma_+(\omega)e^{-\gamma_1(\omega)d_1} & \Gamma_+(\omega) & -\Gamma_-(\omega)\Gamma_+(\omega)e^{-\gamma_1(\omega)d_1} & 1 \end{bmatrix} \quad (26) \end{aligned}$$

This matrix contains every set of transfer functions for the system. For example, the value in row 2 and column 1 represents  $S_{-|1,1|+}(\omega)$ , the transfer function between node 1 (the  $-|1$  interface) and node 2 (the  $1|+$  interface). This is exactly equal to the two-interface reflection coefficient in (4), as derived in Section 2.

#### 4.2. Frequency-Dependent Velocity and Attenuation (Dispersion)

We now simulate a one-dimensional transmission line with frequency-dependent characteristic impedances and velocity characteristics. In this example, we are effectively modeling a transmission line with dispersion [33]. Fig. 5 illustrates the two-interface transmission line that we consider. Fig. 6

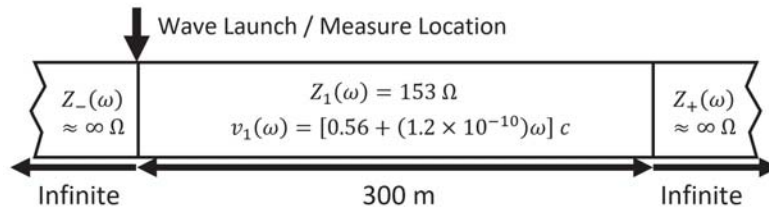


**Figure 5.** Illustration of a one-dimensional, two-interface transmission line with frequency-dependent impedances and velocities.

shows how the attenuation (Fig. 6(a)) and wave velocity (Fig. 6(b)) vary with distance and frequency. The characteristic impedance is relatively constant across frequency at  $Z_1(\omega) = 153 \Omega$ .

Figure 7 illustrates the time-domain impulse response of the reflections at node 1 (i.e., the location of excitation). Fig. 7(a) shows the full simulation, while Fig. 7(b) magnifies the first arrival. In Fig. 7(a), we observe several signal reflections. In Fig. 7(b), we confirm that the high frequencies arrive later (travel slower) than the lower frequencies and observe that the dispersion significantly affects the impulse response.

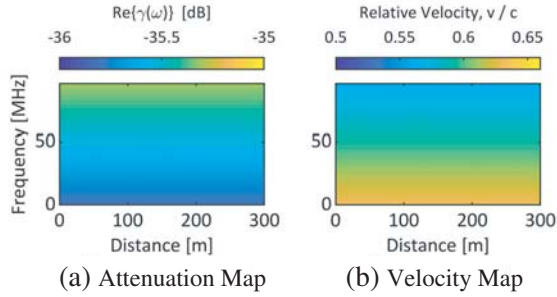


**Figure 6.** The frequency and distance variability for the (a) attenuation and (b) velocity in a two-interface transmission line.

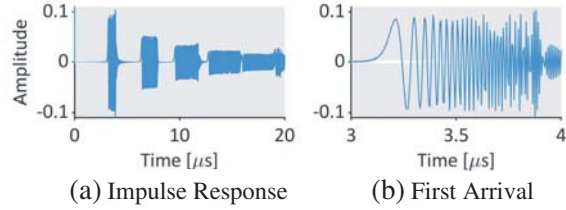


**Figure 7.** The (a) impulse response and (b) magnified impulse response for the two-interface transmission line with frequency-dependent characteristics. This illustrates the resulting velocity dispersion (i.e., lower frequencies travel faster) in the transmission line.

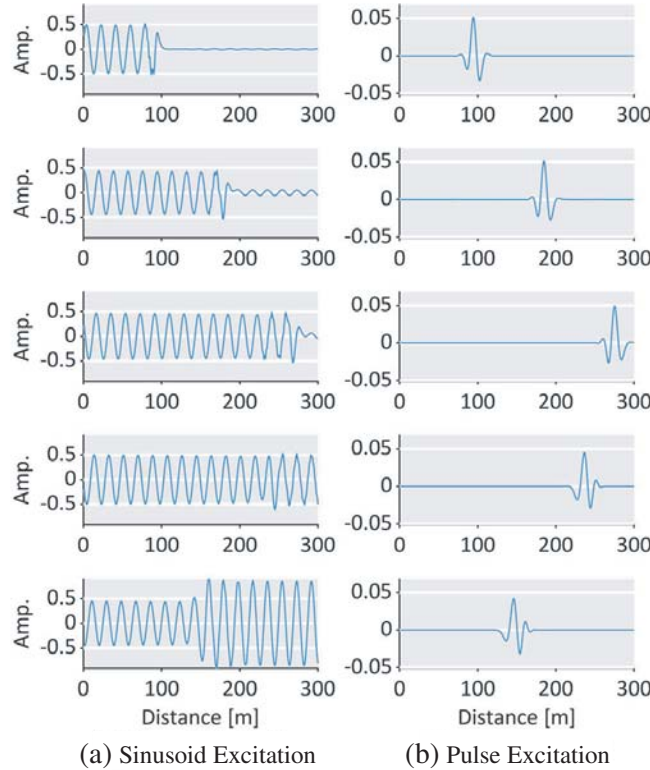


**Figure 8.** Illustration of a wave propagating in a two-interface transmission line with frequency-dependent characteristics. We show two excitations: (a) a 10 MHz sinusoid and (b) a 10 MHz, 10 MHz bandwidth Gaussian pulse. From top-to-bottom, we show five uniformly separated snapshots in time.

Figure 8 illustrates the amplitude of the waves across space. We consider two different excitation signals: a 10 MHz cosine (Fig. 8(a)) and a 10 MHz center frequency, 10 MHz bandwidth Gaussian pulse (Fig. 8(b)). As expected from Fig. 6, we observe the higher frequencies to travel slower with the Gaussian excitation. The cosine excitation is unaffected by velocity dispersion since it has only one frequency. The reflected signal (seen in the fourth and fifth plots) has no change in the polarity since infinite-length segments have an infinite impedance (i.e., an open circuit in transmission line theory).

### 4.3. Multiple Characteristic Impedances

We next demonstrate a simulation with four interfaces. We choose four interfaces since this provides relatively interpretable results. Fig. 9 illustrates the four-interface transmission line. Fig. 10 shows how the characteristic impedance (Fig. 10(a)) and wave velocity (Fig. 10(b)) vary with distance and frequency. The attenuation constant and velocity are both relatively constant across frequency and distance. The first interface is located at the wave excitation location. The remaining 3 interfaces are placed at 60 meters, 150 meters, and 300 meters from the excitation location. As a result, the impedance discontinuities introduce an infinite number of interleaving reflections and transmissions.

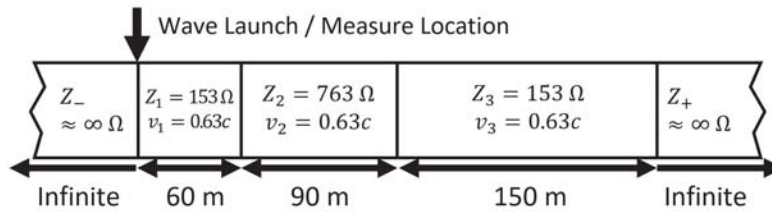


**Figure 9.** Illustration of a one-dimensional, four-interface transmission line.

Figure 11 illustrates the time-domain impulse response of the reflections at node 1. Fig. 11(a) shows the full simulation, while Fig. 11(b) magnifies the first several arrivals. In Fig. 11(a), we confirm that the reflections repeat over time while attenuating. In Fig. 11(b), we confirm that the first two reflections (traveling 120 m and 240 m, to and from the second interfaces) experience no polarity change since they reflect from a higher impedance interface. The third reflection (traveling 300 m, to and from the third interface) experiences a polarity change since it reflects from a lower impedance interface.

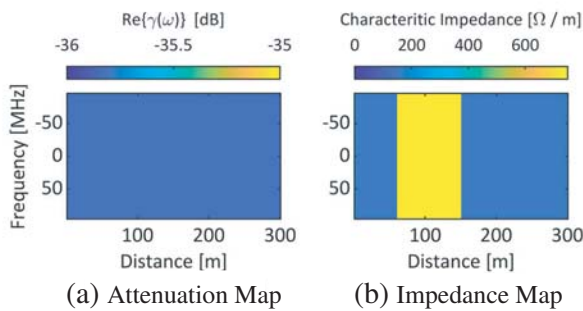


**Figure 10.** The frequency and distance variability for the (a) impedance and (b) velocity in a four-interface transmission line.

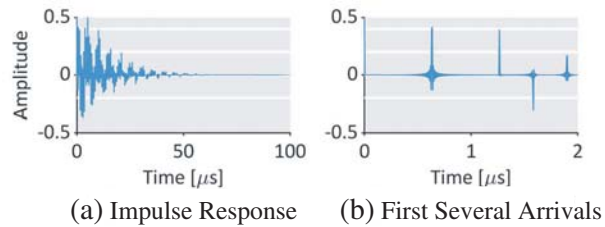


**Figure 11.** The (a) impulse response and (b) magnified impulse response for the four-interface transmission line. This illustrates the resulting multiple reflections from the multiple interfaces.

Figure 12 shows the spatial propagation of a 10 MHz sinusoid (Fig. 12(a)) and a 10 MHz center frequency, 10 MHz bandwidth Gaussian pulse (Fig. 12(b)). Dotted lines are added to the plots to illustrate the impedance boundaries. Fig. 12 illustrates a greater than 1 transmission coefficient when the wave moves from a low impedance ( $\approx 150 \Omega$ ) into a high impedance ( $\approx 750 \Omega$ ). Conversely, the transmission coefficient is weak when transitioning back into the low impedance region ( $\approx 150 \Omega$ ).

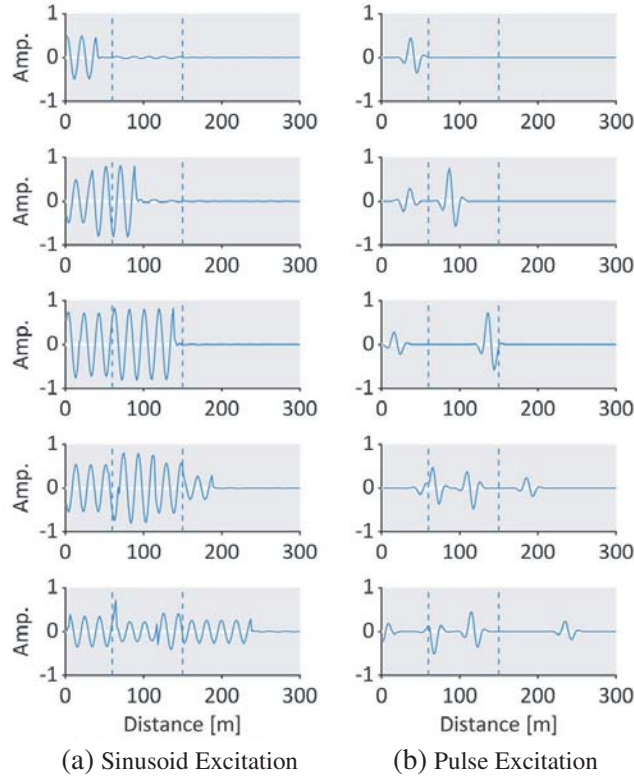


**Figure 12.** Illustration of a wave propagating in a four-interface transmission line. We show two excitations: (a) a 10 MHz sinusoid and (b) a 10 MHz, 10 MHz bandwidth Gaussian pulse. Dashed lines indicate the location of impedance interfaces. From top-to-bottom, we show five uniformly separated snapshots in time.

#### 4.4. Spatially-Dependent Velocity

We finally demonstrate wave propagation in a spatial gradient. Specifically, the velocity slowly varies from approximately  $0.632c$ , where  $c$  is the speed of light, at the left-most end of the transmission line to approximately  $0.16c$  at the right-most end of the transmission line. Unlike the other two examples, the right-most boundary also has an impedance of  $0\Omega$ , a short circuit. Fig. 13 illustrates the transmission line. Fig. 14 shows how the attenuation (Fig. 14(a)) and wave velocity (Fig. 14(b)) vary with distance and frequency. The characteristic impedance is relatively constant across frequency at  $Z_1(\omega) = 153\Omega$ .

Figure 15 illustrates the time-domain impulse response of the reflections at node 1. Fig. 15(a) shows the full simulation while Fig. 15(b) magnifies the first several arrivals. In Fig. 15(a), we see that, although the signal is distorted in space, it remains an impulse in time. This is expected since all variability in the transmission line is spatial. We also observe that the signal polarity repeatedly flips

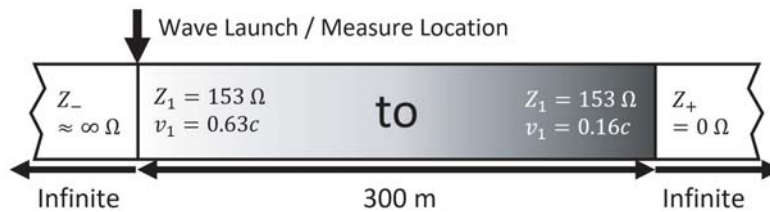


**Figure 13.** Illustration of a one-dimensional, two-interface transmission line with spatially varying velocity characteristics.

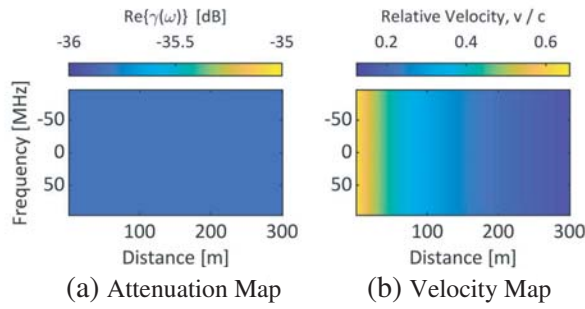


**Figure 14.** The frequency and distance variability for the (a) impedance and (b) velocity in a two-interface transmission line with spatially varying velocity.

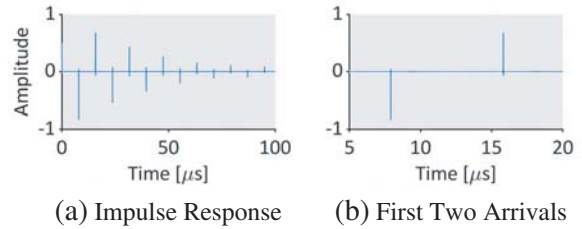


**Figure 15.** The (a) impulse response and (b) magnified impulse response for the two-interface transmission line with spatially varying velocities. This illustrates that the velocity varies with space, but not time.

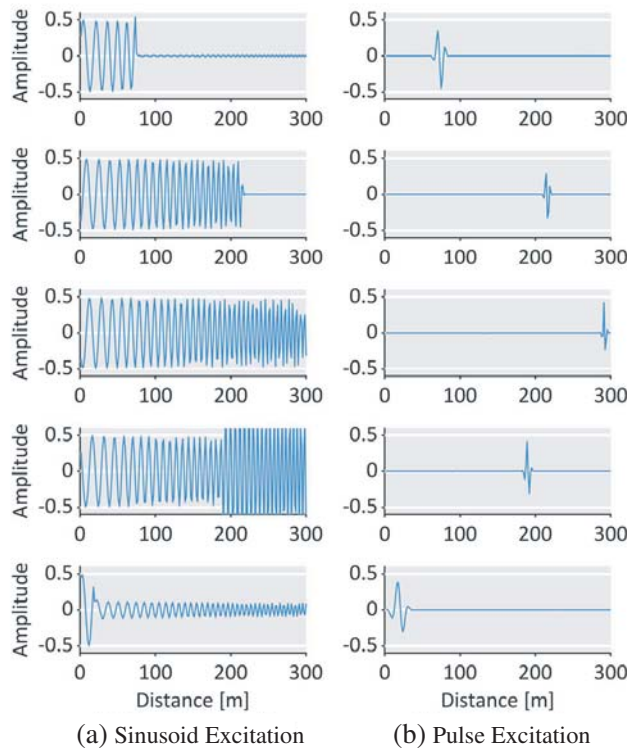


**Figure 16.** Illustration of a wave propagating in a two-interface transmission line with spatially varying velocities. We show two excitations: (a) a 10 MHz sinusoid and (b) a 10 MHz, 10 MHz bandwidth Gaussian pulse. Dashed lines indicate the location of impedance interfaces. From top-to-bottom, we show five uniformly separated snapshots in time.

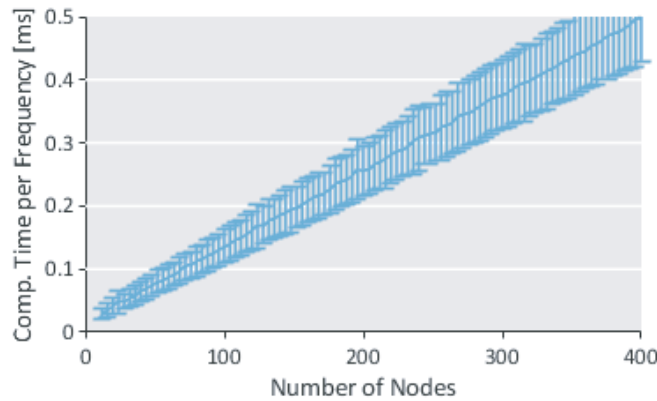
due to the  $0\ \Omega$  impedance at the right-most interface (i.e., reflection coefficient of  $-1$ ).

Figure 16 illustrates the amplitude of the waves across space. We again consider two different excitation signals: a 10 MHz cosine (Fig. 16(a)) and a 10 MHz center frequency, 10 MHz bandwidth Gaussian pulse (Fig. 16(b)). Fig. 16(a) shows how the spatially varying velocity affects a single frequency. The wavelength decreases as the velocity decreases. Fig. 16(b) shows a similar effect. The wave returns to its original wavelength as it travels back to the starting location. We also observe a change in polarity due to the  $0\ \Omega$  impedance at the right-most interface (i.e., reflection coefficient of  $-1$ ).

#### 4.5. Evaluating Computational Complexity

To validate the computational complexity of our engine, we generate  $M$  random transmission lines with  $N$  nodes, or  $N/4$  segments. For each random transmission line, we solve the linear system for  $Q$  different frequencies. Therefore, for each  $N$  considered, we solve the linear system  $MQ$  times. We assess the mean computation time of the trials to measure the computational complexity of our method.

We perform this test with  $M = 100$  and  $Q = 1000$  for a number of nodes ranging from  $N = 12$  to  $N = 400$ . We solve the linear system with the unsymmetric multifrontal method for sparse, non-symmetric matrices that is built into MATLAB 2018a [34]. Fig. 17 illustrates the mean and standard deviation error bars of these trials. The mean values have a clear linear fit ( $R^2 = 0.9999$ ) with respect to the number of nodes. This shows that our approach (for a fixed  $Q$ ) has a computational complexity of  $\mathcal{O}(N)$  and the computational time increases linearly with the number of nodes or interfaces in the transmission line.



**Figure 17.** An illustration of the measured computational time per frequency versus the number of nodes in a transmission line. The error bars indicate one standard deviation in either direction.

## 5. CONCLUSIONS

Algebraic graph theory has been shown to be effective for modeling a wave propagating in a multi-segment transmission line. In our graphical model, the nodes represent the location just before and after a change in the characteristic impedance or propagation coefficient. The edges represent the transition from one node to another. This model represents one-dimensional wave propagation from the reflection and transmission coefficients of each interface and the propagation coefficients of each segment.

The model has a relatively fast computation and low complexity  $\mathcal{O}(N)$  for simulating all reflections and transmissions. We proved that our approach is numerically stable and computational fast. We also demonstrated that the exact solution for a two-interface transmission line matches our numerical approach. We illustrated this engine by simulating three media with various properties.

The results are promising and can be significantly extended. Specifically, the work could be further extended to branching networks. Alternatively, the methods could be used to analyze more complex one-dimensional problems, such as those illustrated by a four- or six-port network.

## ACKNOWLEDGMENT

This material is based upon work supported by the U.S. Department of Energys Office of Energy Efficiency and Renewable Energy (EERE) under Solar Energy Technologies Office (SETO) Agreement Number DE-EE0008169 in collaboration with Livewire Innovation and the National Renewable Energy Laboratory.

## REFERENCES

1. Krautkrämer, J. and H. Krautkrämer, *Ultrasonic Testing of Materials*, Springer Science & Business Media, Apr. 2013.
2. Cawley, P., “Practical guided wave inspection and applications to structural health monitoring,” *Proc. of the Australasian Congress on Applied Mechanics*, 10, Brisbane, Dec. 2007.
3. Moilanen, P., “Ultrasonic guided waves in bone,” *IEEE Trans. Ultrason. Ferroelectr. Freq. Control*, Vol. 55, No. 6, 1277–1286, 2008.
4. Smith, P., C. Furse, and J. Gunther, “Analysis of spread spectrum time domain reflectometry for wire fault location,” *IEEE Sens. J.*, Vol. 5, No. 6, 1469–1478, Dec. 2005.
5. Lowe, M. J. S., “Matrix techniques for modeling ultrasonic waves in multilayered media,” *IEEE Trans. Ultrason. Ferroelectr. Freq. Control*, Vol. 42, No. 4, 525–542, Jul. 1995.
6. Furse, C., P. Smith, C. Lo, Y. C. Chung, P. Pendayala, and K. Nagoti, “Spread spectrum sensors for critical fault location on live wire networks,” *Struct. Control Health Monit.*, Vol. 12, Nos. 3–4, 257–267, Jul. 2005.
7. Santos, E. J. P. and L. B. M. Silva, “Calculation of scattering parameters in multiple-interface transmission-line transducers,” *Measurement*, Vol. 47, 248–254, Jan. 2014.
8. Sumithra, P. and D. Thiripurasundari, “Review on computational electromagnetics,” *Advanced Electromagnetics*, Vol. 6, No. 1, 42–55, Mar. 2017.
9. Chakraborty, A. and S. Gopalakrishnan, “A spectrally formulated finite element for wave propagation analysis in layered composite media,” *Int. J. Solids Struct.*, Vol. 41, No. 18, 5155–5183, Sep. 2004.
10. Alterman, Z. and F. C. Karal, “Propagation of elastic waves in layered media by finite difference methods,” *Bulletin of the Seismological Society of America*, Vol. 58, No. 1, 367–398, Feb. 1968.
11. Hoefler, W. J. R., “The transmission-line matrix method — Theory and applications,” *IEEE Trans. Microw. Theory Tech.*, Vol. 33, No. 10, 882–893, Oct. 1985.
12. Bohlen, T. and E. Saenger, “Accuracy of heterogeneous staggered-grid finite-difference modeling of Rayleigh waves,” *Geophysics*, Vol. 71, No. 4, T109–T115, Jul. 2006.
13. Liu, T., C. Zhao, and Y. Duan, “Generalized transfer matrix method for propagation of surface waves in layered azimuthally anisotropic half-space,” *Geophysical Journal International*, Vol. 190, No. 2, 1204–1212, Aug. 2012.
14. Katsidis, C. C. and D. I. Siapkas, “General transfer-matrix method for optical multilayer systems with coherent, partially coherent, and incoherent interference,” *Appl. Opt.*, Vol. 41, No. 19, 3978–3987, Jul. 2002.
15. Troparevsky, M. C., A. S. Sabau, A. R. Lupini, and Z. Zhang, “Transfer-matrix formalism for the calculation of optical response in multilayer systems: From coherent to incoherent interference,” *Opt. Express*, Vol. 18, No. 24, 24 715–24 721, Nov. 2010.
16. Cormen, T. H., C. E. Leiserson, R. L. Rivest, and C. Stein, *Introduction to Algorithms*, MIT Press, 2009.
17. Farmaga, I., P. Shmigelskyi, P. Spiewak, and L. Ciupinski, “Evaluation of computational complexity of finite element analysis,” *Proc. of the International Conference The Experience of Designing and Application of CAD Systems in Microelectronics*, 213–214, Feb. 2011.
18. Davidson, D. B. and R. W. Ziolkowski, “Body-of-revolution finite-difference time-domain modeling of space-time focusing by a three-dimensional lens,” *J. Opt. Soc. Am. A, JOSAA*, Vol. 11, No. 4, 1471–1490, Apr. 1994.
19. Pozar, D. M., *Microwave Engineering*, 4th Edition, Wiley, Nov. 2011.
20. Mason, S. J., “Feedback theory — Some properties of signal flow graphs,” *Proceedings of the IRE*, Vol. 41, No. 9, 1144–1156, Sep. 1953.
21. Schutt-Aine, J. E., “Transient analysis of nonuniform transmission lines,” *IEEE Transactions on Circuits and Systems I: Fundamental Theory and Applications*, Vol. 39, No. 5, 378–385, May 1992.

22. Acar, C., “Nth-order voltage transfer function synthesis using a commercially available active component: Signal-flow graph approach,” *Electron. Lett.*, Vol. 32, No. 21, 1933–1934, Oct. 1996.
23. Biggs, N., N. L. Biggs, and E. N. Biggs, *Algebraic Graph Theory*, Cambridge University Press, 1993, Vol. 67.
24. Li, Z., Z. Duan, G. Chen, and L. Huang, “Consensus of multiagent systems and synchronization of complex networks: A unified viewpoint,” *IEEE Transactions on Circuits and Systems I: Regular Papers*, Vol. 57, No. 1, 213–224, Jan. 2010.
25. Sezer, M. E. and D. D. iljak, “Nested-decompositions and clustering of complex systems,” *Automatica*, Vol. 22, No. 3, 321–331, 1986.
26. George, A., J. R. Gilbert, and J. W. Liu, *Graph Theory and Sparse Matrix Computation*, Vol. 56, Springer Science & Business Media, 2012.
27. Dhillon, I. S. and D. S. Modha, “Concept decompositions for large sparse text data using clustering,” *Machine Learning*, Vol. 42, Nos. 1–2, 143–175, 2001.
28. Shuman, D. I., S. K. Narang, P. Frossard, A. Ortega, and P. Vandergheynst, “The emerging field of signal processing on graphs: Extending high-dimensional data analysis to networks and other irregular domains,” *IEEE Signal Processing Magazine*, Vol. 30, No. 3, 83–98, May 2013.
29. Sandryhaila, A. and J. M. Moura, “Big data analysis with signal processing on graphs: Representation and processing of massive data sets with irregular structure,” *IEEE Signal Processing Magazine*, Vol. 31, No. 5, 80–90, 2014.
30. Puschel, M. and J. M. F. Moura, “Algebraic signal processing theory: Foundation and 1-D time,” *IEEE Trans. Signal Process.*, Vol. 56, No. 8, 3572–3585, Aug. 2008.
31. Davis, T. A., S. Rajamanickam, and W. M. Sid-Lakhdar, “A survey of direct methods for sparse linear systems,” *Acta Numerica*, Vol. 25, 383–566, 2016.
32. Bunch, J. R. and D. J. Rose, *Sparse Matrix Computations*, Academic Press, 2014.
33. Luebbers, R., F. P. Hunsberger, K. S. Kunz, R. B. Standler, and M. Schneider, “A frequency-dependent finite-difference time-domain formulation for dispersive materials,” *IEEE Trans. Electromagn. Compat.*, Vol. 32, No. 3, 222–227, Aug. 1990.
34. Davis, T. A., “Algorithm 832: UMFPACK v4.3 — An unsymmetric-pattern multifrontal method,” *ACM Trans. Math. Softw.*, Vol. 30, No. 2, 196–199, Jun. 2004.